Department of Biotechnology[1], Federal University of São João del-Rei, Divinópolis; School of Pharmacy[2], Federal University of Ouro Preto, Chemistry Department[3]; Department of Metallurgical and Materials Engineering[4], Federal University of Minas Gerais, Belo Horizonte; Center of Research in Biological Chemistry[5], Federal University of São João del-Rei, Divinópolis, Minas Gerais, Brazil.

Spiramyin-loaded PLGA implants for the treatment of ocular toxoplasmosis: development, characterization, biocompatibility, and anti-toxoplasma activity

H. S. Tavares[1], J. F. Cardoso[2], T. C. Almeida[2], M. B. F. Marques[3], W. N. Mussel[3], M. C. P. Lopes[1], R. L. Oréfice[4], S. N. Andrade[5], F. P. Varotti[5], G. N. Silva[2], G. R. Da Silva[2,*]

Received July 23, 2020, accepted November 14, 2020

**Corresponding author: Gisele Rodrigues Da Silva (GR Da Silva). Federal University of Ouro Preto, Morro do Cruzeiro w/n, Bauxita, 35.400-000, Ouro Preto, Minas Gerais, Brazil. giselersilva@ufop.edu.br*

Pharmazie 76: 68-76 (2021) *doi: 10.1691/ph.2021.0100*

Ocular toxoplasmosis is the major cause of infectious posterior uveitis worldwide, inducing visual field defect and/or blindness. Despite the severity of this disease, an effective treatment is still lacking. In this study, spiramycin-loaded PLGA implants were developed aiming at the treatment of ocular toxoplasmosis. Implants were manufactured by a hot-molding technique, characterized by Fourier Transform Infrared Spectroscopy, X-Ray Diffraction, Differential Scanning Calorimetry, Scanning Electron Microscopy; evaluated in terms of ocular biocompatibility by immunofluorescence, flow cytometry, cell migration, Hen's egg test-chorioallantoic membrane (HET-CAM) irritation test; and investigated in terms of *in vitro* efficacy against *Toxoplasma gondii*. Characterization techniques indicated that spiramycin was dispersed into the polymeric chains and both substances preserved their physical structures in implants. The HET-CAM test indicated that implants did not induce hemorrhage or coagulation, being non-irritant to the CAM. ARPE-19 cells showed viability by MTT assay, and normality in cell cycle kinetics and morphology, without stimulating cell death by apoptosis. Finally, they were highly effective against intracellular parasites without inducing human retinal pigment epithelial cell death. In conclusion, spiramycin-loaded PLGA implants represent a promising therapeutic alternative for the local treatment of ocular toxoplasmosis.

1. Introduction

Toxoplasmosis is caused by *Toxoplasma gondii*, a protozoan parasite of Apicomplexa phylum, capable of attaching itself to the host cell membrane through its polar apical complex (Ozgonul and Besirli 2016). Approximately one-third of the world's population are infected with *Toxoplasma gondii* (Maenz et al. 2014). In addition, seroprevalence varies from 10 to 80% among countries and within countries. Southeast Asia, North America, and Northern Europe report 10-30% of seroprevalence, indicating the lowest level worldwide (Dubey and Jones 2008; Ozgonul and Besirli 2016). Central and Southern Europe register 30-50% of seroprevalence, whereas Latin America and tropical African countries present the highest seroprevalences (Robert-Gangneux and Dardé 2012; Ozgonul and Besirli 2016). The reason for the differences in seroprevalence is probably related to the existence of cysts and oocysts of the parasite in the environment (Pappas et al. 2009).

Ocular toxoplasmosis manifests itself in approximately 2% of the clinically confirmed cases of infection (Petersen et al. 2012). Ocular toxoplasmosis causes toxoplasmic retinochoroiditis, vitritis, and less frequently, damages to macula and/or the optic nerve. Visual loss may become permanent due to the recurrence of the infection, inducing the formation of scars in the macula and/or optic atrophy (Kim et al. 2013). In immunocompetent patients, toxoplasmic retinochoroiditis is generally a self-limited infection and may resolve spontaneously within 6 to 8 weeks (Brydak-Godowska et al. 2015). However, medication is recommended when lesions are adjacent to the optic disk or larger than two optic disc diameters, and within the large vascular arcades. In these conditions, the risk of visual loss is high. In immunocompromised patients, toxoplasmic retinochoroiditis has to be immediately treated (Holland and Lewis 2002).

Treatment of ocular toxoplasmosis involves the administration of macrolide antibiotics, sulfonamides, and pyrimethamine. The oral combination of sulfadiazine, pyrimethamine, and folinic acid can inhibit the growth of *Toxoplasma gondii* in the proliferative stage. However, pyrimethamine can cause bone marrow depression, skin and gastrointestinal side effects; and sulfadiazine may cause anaphylaxis. When patients experienced significant side effects after administering the combination of sulfadiazine and pyrimethamine, or a drug-resistant parasite is confirmed, other antibiotics such as spiramycin, clindamycin, and azithromycin are used for the treatment of infections by *Toxoplasma*. Spiramycin is the first-choice drug in pregnant women, since it is effective against the parasite, without inducing teratogenicity (Brydak-Godowska et al. 2015; Xiaoli and Yu, 2018).

Despite the therapeutic schemes for the treatment of ocular toxoplasmosis being well-established, failures occur, not only due to drug intolerance, poor compliance, and the resistance of parasites, but also to the low drug bioavailability in the posterior segment of the eye, since the blood-retinal barrier prevents the penetration of therapeutic doses of drugs into the eye cavity (Fernandes-Cunha et al. 2016). As a result of this scenario, severe visual field defects may be developed. Therefore, achieving therapeutic anti-*Toxoplasma* drug concentrations in the eye is essential to prevent the ocular manifestations of toxoplasmosis and, consequently, visual damage.

Ocular implantable polymeric devices represent a therapeutic alternative for the local treatment of ocular toxoplasmosis, since they are inserted directly in the posterior segment of the eye, overcoming ocular barriers and improving drug pharmacokinetics. In addition, implants can control and prolong drug release in the target tissues, which induce direct drug contact with the parasites for a longer period, reducing/eliminating the parasitemia and avoiding resistance. Finally, implants can prolong drug action for months to years by using reduced doses of the incorporated drug when compared to the doses in conventional pharmaceutical dosage forms. Dose reduction results in reduced or no side effects and/or toxicity, enhancing patient compliance, and, consequently, improving pharmacological responses (Silva et al. 2020).

Currently, intravitreal implants are commercially available for the treatment of non-infectious uveitis (Retisert®, Bausch & Lomb, Inc., USA), diabetic macular edema (Iluvien®, Alimera Sciences, Inc., USA), and non-infectious posterior uveitis and retinal vein occlusion (Ozurdex®, Allergan, USA) (Gote et al. 2019). By contrast, polymeric implantable devices containing clindamycin, aiming at the treatment of ocular toxoplasmosis, were developed (Fernandes-Cunha et al. 2016, 2017; Tamaddon et al. 2015); but progress in clinical trials has not been achieved. Therefore, more investigation is necessary to transfer these implants to affected patients.

With this scenario in mind, in this study, spiramycin-loaded PLGA implants were developed for the treatment of ocular toxoplasmosis. These implants were composed of poly(lactic-*co*-glycolic) acid (PLGA), a biodegradable and biocompatible polymer, capable of controlling and prolonging the release of spiramycin. Besides the well-established anti-*Toxoplasma* activity, spiramycin also shows anti-inflammatory activity, since it is capable of modulating the expression of pro-inflammatory cytokines and inhibiting the chemotaxis and inflammatory cell infiltration (Brydak-Godowska et al. 2015). Therefore, spiramycin can simultaneously contribute to eliminate the parasite and suppress the inflammatory process established in the infected ocular tissues. Implants were developed by a hot-molding technique and characterized by different analytical instrumental techniques. In addition, the *in vitro* biocompatibility of spiramycin-loaded PLGA implants was also evaluated by immunofluorescence, flow cytometry, HET-CAM test, and *in vitro* anti-*Toxoplasma* activity. Finally, spiramycin-loaded PLGA implants represent a novel ocular drug delivery system able to simultaneously suppress infection and inflammation, which characterize toxoplasmic retinochoroiditis, established in ocular toxoplasmosis.

2. Investigations and results

2.1. Development of spiramycin-loaded PLGA implants

Spiramycin-loaded PLGA implants were developed by a hot molding technique. Spiramycin and PLGA 85:15 were dissolved in acetonitrile to form a molecular mixture of substances. Subsequently, the acetonitrile was evaporated and the combined powder was molded under heating. The melting of the polymer propitiated the entrapment of spiramycin into the polymeric chains. Spiramycin-loaded PLGA implants were molded as cylinders measuring 0.90±0.05 mm in diameter, 3.00±0.22 mm in length, and 3.00±0.15 mg in average weight (n = 10). The content of spiramycin in the PLGA implants was 99.73±1.60% (n = 10).

2.2. Characterization

2.2.1. Fourier Transform Infrared Spectroscopy (FTIR)

Figure 1 represents the FTIR spectra of PLGA 85:15 (Fig. 1A), spiramycin (Fig. 1B), and spiramycin-loaded PLGA implants (Fig. 1C). The FITR spectrum of PLGA 85:15 showed bands at 1760 cm^{-1} (C=O stretch from ester), 1090-1185 cm^{-1} (C-O stretch from ester), and 2995 cm^{-1} (C-H stretch). The infrared spectrum of spiramycin demonstrated bands at 1724 cm^{-1} (O=C-O-H stretch), 2785-2970 cm^{-1} (C-H stretch), and 3470 cm^{-1} (C-OH stretch). The FTIR spectrum of spiramycin-loaded PLGA implants showed that the absorption bands attributed to pure PLGA 85:15 and spiramycin were preserved after manufacturing the implantable device; and bands at 1760 and 1724 cm^{-1}, attributed to functional organic groups of PLGA 85:15 and spiramycin, respectively, overlapped.

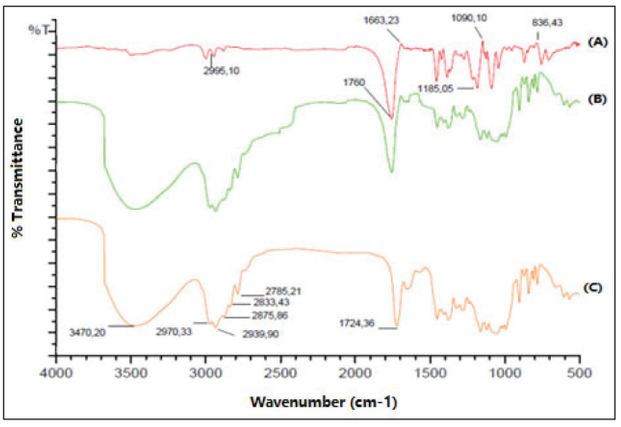

Fig. 1: FTIR spectra of (A) PLGA 85:15, (B) spiramycin, and (C) spiramycin-loaded PLGA implants.

2.2.2. Powder X-Ray Diffraction (XRD)

Figure 2 shows the XRD of PLGA 85:15 (Fig. 2A), spiramycin (Fig. 2B), and spiramycin-loaded PLGA implants (Fig. 2C). The XRD pattern of PLGA 85:15 exhibited two sharp peaks at approximately 2Θ = 16° and 18°, demonstrating its semi-crystalline nature. The XRD pattern of spiramycin revealed a broad peak at approximately 2Θ = 20°, indicating its amorphous structure. XRD diffractogram of spiramycin-loaded PLGA implants indicated that the physical structure of the polymer was preserved, since the sharp peaks corresponding to this substance were detected (2Θ = 16° and 18°). However, the broad peak equivalent to the spiramycin may be overlapped by the other peaks of the PLGA, since it was not detected.

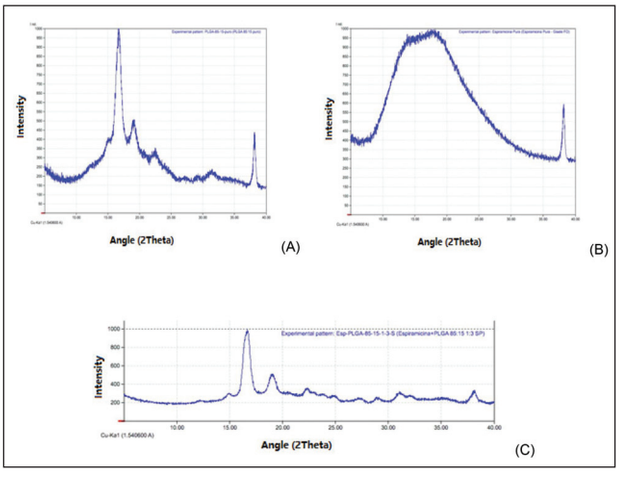

Fig. 2: XRD thermograms of (A) PLGA 85:15, (B) spiramycin, and (C) spiramycin-loaded PLGA implants. Peak at 2Θ = 38° represents the aluminum sample holder.

2.2.3. Thermal analysis

Figure 3 depicts the DSC thermograms of PLGA 85:15, spiramycin, and spiramycin-loaded PLGA implants. The DSC thermogram of PLGA exhibited three endothermic events: at 61.9 °C (ΔH = 2.9 J g-1), corresponding to the polymeric glass transition temperature; at 149.1 °C (ΔH = 14,3 J.g^{-1}), equivalent to the evaporation of lactide monomer; and at 267 °C (ΔH = 507.1 J g-1), corresponding to the polymeric

decomposition. The mass loss of these events was approximately 98%. The DSC curve of spiramycin showed three endothermic events: at about 31–79 °C (ΔH = 13.18 J g^{-1}), followed by 2% of mass loss, indicating the volatilization of residual water; at 110.4 °C (ΔH = 3.09 J g^{-1}), representing drug melting; and at 221–294 °C and at 296 °C, indicating the first and the second decomposition steps, respectively, with a total mass loss of about 92% across all the analyzed temperature range. DSC thermogram of spiramycin-loaded PLGA implants exhibited two endothermic events: between 120 °C and 160 °C, suggesting the overlapping of drug melting and lactide monomer evaporation; and from 280 °C to 300 °C, representing the overlapping of the decomposition of PLGA and spiramycin. The glass transition temperature of the PLGA was not detected.

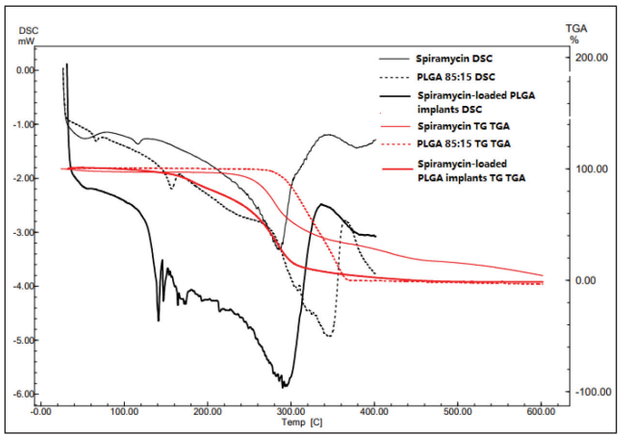

Fig. 3: DSC thermograms of PLGA 85:15, spiramycin, and spiramycin-loaded PLGA implants.

2.2.4. *Scanning Electron Microscopy (SEM)*

Figure 4 shows the SEM images of spiramycin-loaded PLGA implants recently prepared (day zero) and submitted to the simulated physiological ocular conditions for 60 days. On day zero, implants had an irregular and rough surface, consisting of tangled fibers (Fig. 4A and 4B). The transversal section of the implant showed a dense mass, in which polymer and drug cannot be distinguished (Fig. 4C). After 60 days in PBS pH 7.4, implants were deformed (Fig. 4D), indicating its mass loss; and fissures had formed (Fig. 4E).

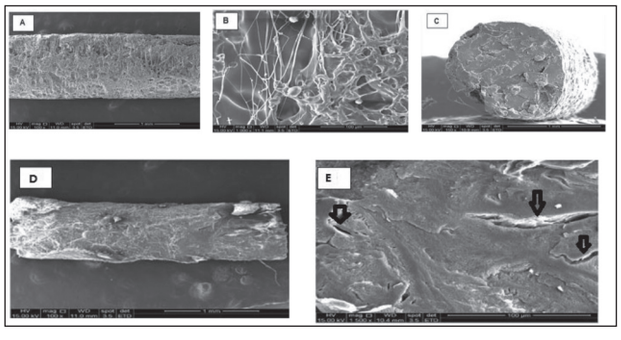

Fig. 4: SEM photomicrographs of (A, B and C) spiramycin-loaded PLGA implants recently prepared (zero day) and (D and E) spiramycin-loaded PLGA implants submitted to drug release conditions (PBS pH 7.4) for 60 days. Arrows indicate fissures. A, C and D – 100× magnification. B and E - 1000× magnification.

2.3. *In vitro release of spiramycin from PLGA implants*

Figure 5 shows the *in vitro* release profile of spiramycin from PLGA implants. In the first two days, approximately 50% of the drug was quickly released in the medium, demonstrating a burst release. From day 2 to day 42, almost 100% of spiramycin released from polymeric implants was controlled in a prolonged manner.

Data on *in-vitro* spiramycin release from PLGA implants were fitted into Higuchi, zero-order, first-order, and Korsmeyer-Peppas equations; and the correlation coefficients (R^2) are described in Table 1. Regarding these values, the implants followed the Korsmeyer-Peppas model, since the correlation coefficient was the highest when compared to those obtained in the other mathematical models. In addition, the diffusional exponent (n) was calculated. The n value was equal to 1.50, indicating the super-case II transport.

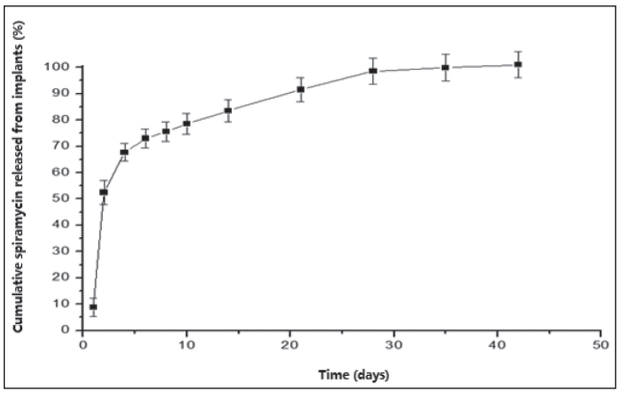

Fig. 5: *In vitro* spiramycin release profile from PLGA implants. Data were expressed as cumulative percentage of released spiramycin ± standard deviation (n = 5).

Table 1: Correlation coefficients (R^2) obtained by using different mathematical models to describe the spiramycin release kinetic profile from PLGA implants. The diffusional exponent (n) for Korsmeyer-Peppas was also expressed

Correlation coefficient (R^2)			
Higuchi	**Zero order**	**First order**	**Korsmeyer-Peppas**
0.8950	0.5920	0.9984	0.9998 (n = 1.50)

2.4. *In vitro biocompatibility study*

2.4.1. *Cytotoxicity of spiramycin released from PLGA implants*

The viability of ARPE-19 cells in the control medium (fixed as 100%) and in direct contact with spiramycin and polymeric degradation products released from PLGA implants for 4 and 8 days (92.31±0.76% and 90.08±0.24%, respectively) did not show a statistical difference ($p < 0.05$), demonstrating the absence of cytotoxic effects (Fig. 6).

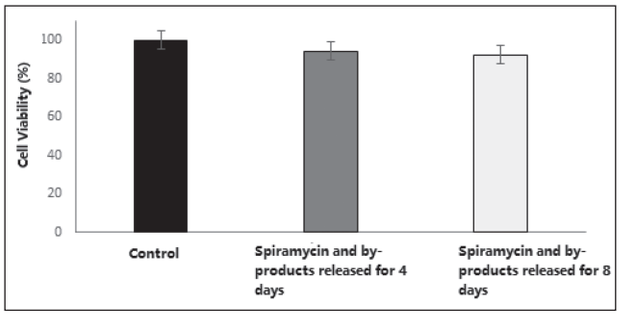

Fig. 6: ARPE-19 viability in contact with spiramycin and polymeric by-products released from PLGA implants for 4 and 8 days. Cell viability on control medium was fixed as 100%. Viability was determined by MTT assay. Data represented mean±standard deviation (n = 10 for each sample at each time).

2.4.2. *Cell cycle kinetic*

ARPE-19 cells in direct contact with spiramycin and polymeric by-products released from PLGA implants for 4 and 8 days were analyzed by flow cytometry regarding the cell cycle progression.

Table 2: Percentages of ARPE-19 cells in G0/G1, S, and G2/M phases after 48 hours in contact with spiramycin and polymeric by-products released from PLGA implants for 4 and 8 days. Control represented ARPE-19 cells in the culture medium without treatment. ($p < 0.05$)

	G0/G1	S	G2/M
Control (4 days)	66.40 ± 1.37	8.80 ± 0.71	24.20 ± 1.42
Spiramycin and polymeric by-products released for 4 days	60.03 ± 1.05	8.92 ± 1.10	30.43 ± 1.58
Control (8 days)	58.97 ± 1.94	9.87 ± 0.32	30.57 ± 2.08
Spiramycin and polymeric by-products released for 8 days	59.60 ± 0.98	10.23 ± 2.48	29.63 ± 2.70

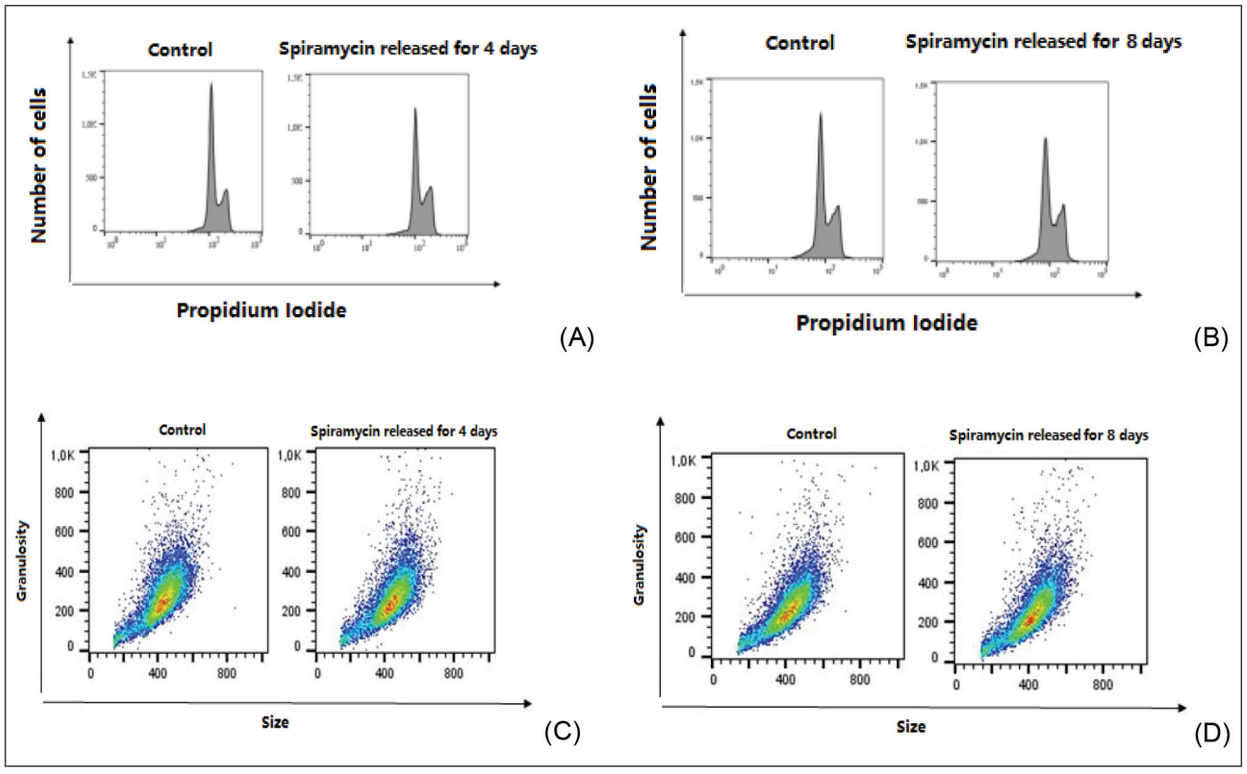

Fig. 7: Effect of spiramycin and polymeric by-products released from PLGA implants for 4 (A and C) and 8 (B and D) days on G0/G1, S, and G2/M phases, and granulosity. Sub-G1 phase was undetectable. ARPE-19 cells were incubated for 48 hours and stained with propidium iodide. Data represent mean of triplicate.

Percentages of ARPE-19 control and cells exposed to spiramycin and polymeric by-products in G0/G1, S, and G2/M phases did not statistically differ ($p < 0.05$), suggesting that the cell cycle progression was not disturbed by implants. In addition, implants did not stimulate cell death by apoptosis, since sub-G1 phase content was not observed. Finally, the size and granulosity of ARPE-19 cells were also evaluated after exposition by spiramycin and polymeric by-products; and they did not promote modifications in morphological parameters when compared to control cells. Data on cell cycle kinetics and cell morphology are described in Table 2 and Fig. 7.

2.4.3. Cell migration (In vitro wound-healing assay)

Effects of spiramycin and polymeric degradation products released from PLGA implants for 4 and 8 days on the ARPE-19 cell migration were evaluated by the *in vitro* wound-healing assay. After 48 and 72 hours of incubation, ocular cells in direct contact with spiramycin and by-products lixiviated from PLGA implants for 4 days showed migration comparable to the control cells ($p < 0.05$). In addition, after 48 hours of incubation, substances released from polymeric implants for 8 days did not interfere on ARPE-19 cell migration; however, after 72 hours of incubation, they increased cell migration compared to the control cells ($p > 0.05$). Migration percentages are described in Table 3.

2.5. Hen's egg test-chorioallantoic membrane (HET-CAM) irritation test

Figure 8 shows that spiramycin and polymeric by-products released from PLGA implants for 4 and 8 days (Fig. 8A and 8B) did not induce hyperemia, hemorrhage, and coagulation on the CAM surface over the period of 5 min. By contrast, 0.1 mol/L sodium hydroxide solution (positive control) promoted vessel lysis and hemorrhage (Fig. 8C), inducing irritation to the CAM.

Table 3: Percentages of ARPE-19 cell migration after 48 and 72 hours in contact with spiramycin and polymeric degradation products released from PLGA implants for 4 and 8 days. Control represented ARPE-19 cells in the culture medium without treatment. *($p > 0.05$)

	48 hours	72 hours
Control (4 days)	61.83 ± 1.05	71.41 ± 0.43
Spiramycin and polymeric by-products released for 8 days	55.84 ± 0.70	73.50 ± 1.12
Control (8 days)	45.96 ± 2.35	36.25 ± 0.27
Spiramycin and polymeric by-products released for 8 days	62.44 ± 1.47	52.79 ± 1.07*

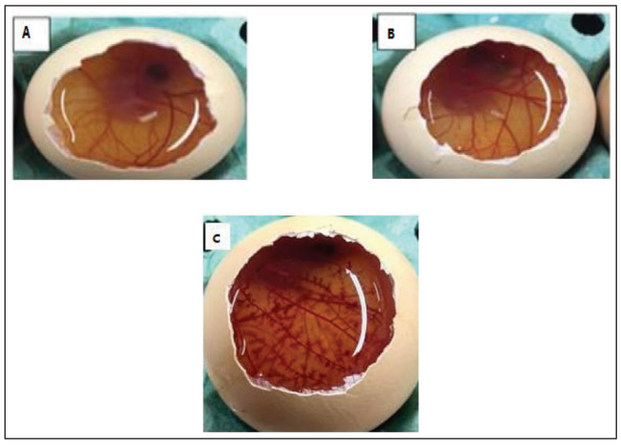

Fig. 8: HET-CAM test: vascular response post-application of (A and B) spiramycin and polymeric by-products released from PLGA implants for 4 and 8 days, respectively, and (C) 0.1 mol/L sodium hydroxide solution (positive control). Implants did not induce vascular phenomena onto the CAM. Positive control was irritant to the CAM.

2.6. Anti-Toxoplasma activity of spiramycin released from PLGA implants

Anti-*Toxoplasma* activity of spiramycin and polymeric by-products released from PLGA implants was determined by measuring the MTT metabolization by ARPE-19 cells infected with *Toxoplasma gondii*. Ocular cells showed approximately 85% and 90% of viability when in direct contact with spiramycin and degradation products lixiviated from polymeric implants for 4 and 8 days, respectively. The statistical analysis revealed no significant difference between treated and untreated cells ($p < 0.05$), suggesting the effectiveness of the implantable devices against intracellular *Toxoplasma gondii*. In addition, the anti-*Toxoplasma* activity of spiramycin at 6.5 and 21.6 µg mL^{-1} was also evaluated. These concentrations are equivalent to those released from PLGA implants after 4 and 8 days in incubation. The spiramycin in solution at both concentrations did not prevent the reduction of ARPE-19 viability when compared to that obtained for the control and treated cells with implants ($p > 0.05$) (Fig. 9).

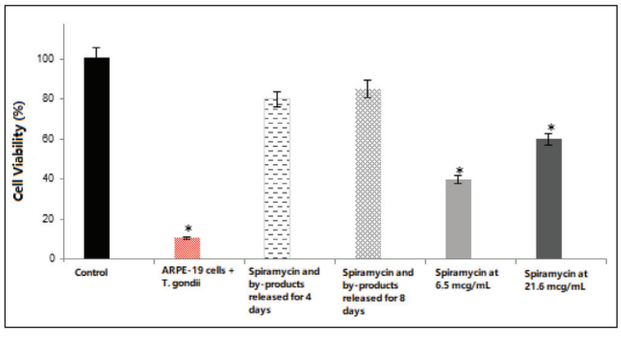

Fig. 9: Viability of ARPE-19 cells infected by *Toxoplasma gondii* after 48 hours of treatment with spiramycin and polymeric by-products released from PLGA implants for 4 and 8 days, and pure spiramycin in solution at 6.5 and 21.6 µg mL^{-1}. Cell viability on control medium was fixed as 100%. Viability was determined by MTT assay. Data represented mean ± standard deviation (n = 10 for each sample at each time or concentration) $^{*}(p > 0.05)$.

2.7. Conclusion

In this study, spiramycin-loaded PLGA implants were developed aiming at the local treatment of ocular toxoplasmosis. These implantable devices showed reduced dimensions (0.90 mm and 3.00 mm in diameter and length, respectively), being possible to inject them into the vitreous cavity by using extremely fine needles. The manufacturing process of implantable devices provided the dispersion of the amorphous spiramycin throughout the semi-crystalline structure of the PLGA 85:15; and they probably established weak chemical interactions, which did not interfere in the controlled drug release from PLGA implants for a prolonged period. Spiramycin-loaded PLGA implants, as a sustained intraocular drug delivery system, did not disturb the ARPE-19 cells genetically, morphologically, and biochemically, indicating their ocular biocompatibility; and this was also demonstrated in the anti-*Toxoplasma* activity test, since implants eliminated the intracellular parasites without reducing the viability of ARPE-19 cells. Finally, spiramycin-loaded PLGA implants showed to be non-irritant to the CAM; and this result was very important, since the HET-CAM test is a borderline case between *in vitro* and *in vivo* experiments. In conclusion, these promising results encourage us to hypothesize that spiramycin-loaded PLGA implants could be a therapeutic alternative to simultaneously suppress *Toxoplasma gondii* and inflammation established in ocular toxoplasmosis.

3. Discussion

Ocular toxoplasmosis is caused by *Toxoplasma gondii*, in which bradyzoites establish cysts in the retina. These cysts are activated by unknown mechanisms, leading not only to retinochoroiditis but also vasculitis, vitritis, and even anterior uveitis (Tabuenca del Barrio et al. 2019). Signs of active ocular toxoplasmosis include retinal inflammatory infiltration followed by disruption of photoreceptors and retinal pigment epithelial cells, detachment of retinal sites, and the thickening of choroid. As a result, in the center of the injured site, an atrophic retina and choroid usually manifest, causing disturbances in vision and significant vision loss (Garweg 2016). Frequently, ocular toxoplasmosis lesions are associated with adjacent old scars, indicating a recurrent infection (Maenz et al. 2014).

Pyrimethamine and trimethoprim, two major drugs in the treatment of ocular toxoplasmosis, must be associated with sulfonamides, to guarantee the synergistic action against the DNA synthesis of parasites by inhibiting the folate pathway (Konstantinovic et al. 2019). However, these combined drugs can cause severe systemic side effects, inducing discontinuation of therapy and the modification of pharmacological regimen. Thus, other antibiotics should be administered such as spiramycin, sulfamethoxazole, clindamycin, and atovaquone; and the treatment needs to be continued for at least 4 to 6 weeks (Maenz et al. 2014), which probably causes systemic side effects, leading to the lack of patient compliance (Brydak-Godowska et al. 2015; Xiaoli and Yu 2018). Finally, after having defined an appropriate oral therapeutic scheme for the patient aiming at the treatment of ocular toxoplasmosis, the full pharmacological potential of these drugs may not be achieved due to low ocular penetration, and consequently, low bioavailability. The blood-retinal barrier restricts the vitreous and retinal distribution of active principles from the systemic circulation (Pascual-Pasto et al. 2017).

Currently, intravitreal injections have been applied as an attempt to treat ocular toxoplasmosis, since they deliver therapeutic doses of drugs directly to the posterior segment of the eye, overcoming the blood-retinal barrier and avoiding systemic side effects. In a clinical study, patients with ocular toxoplasmosis received intravitreal injections of clindamycin and dexamethasone for four weeks. The majority of patients experienced resolution and no recurrences of ocular toxoplasmosis for 24 months (Lasave et al. 2010). However, intravitreal injections are associated with fast drug clearance, resulting in repeated administrations, which may cause retinal detachment and vitreous hemorrhage, among other complications (Khine et al. 2020).

To overcome the drawbacks of conventional pharmaceutical dosage forms, new drug delivery systems, such as intraocular implants, have been developed to deliver active principles directly to the posterior segment of the eye, to improve pharmacokinetics and to avoid systemic side effects (Fernandes-Cunha et al. 2017; De Souza et al. 2016; Saliba et al. 2016). In addition, ocular implantable devices can be produced by using non-biodegradable

or biodegradable polymers that are able to incorporate drugs and release them for a prolonged period, over weeks or months, in a controlled manner. Increased drug residence time improves patient compliance due to the reduced frequency of administration and effectiveness of the therapy.

In this study, spiramycin-loaded PLGA implants were developed as a therapeutic alternative for the local treatment of ocular toxoplasmosis. PLGA was selected to compose the implants since it has considerable mechanical strength, allowing it to be manufactured as drug delivery systems. PLGA is capable of entrapping drug molecules into its polymeric chains, providing controlled drug release for a prolonged time. In addition, it is a biodegradable polymer, and its hydrolytic cleavage generates two monomers (lactic and glycolic acids), which are endogenous substrates of the Krebs cycle, being eliminated from the body as carbon dioxide and water. Finally, PLGA is biocompatible and safe for ocular tissues, being used in ophthalmological applications. In this context, implants based on PLGA and dexamethasone (Ozurdex, Allergan, Inc) are commercially available for the treatment of non-infectious uveitis, central retinal vein occlusion, and macular edema related to retinal vein occlusion. Spiramycin, a macrolide antibiotic, acts against *Toxoplasma gondii* by binding to the 50S ribosomal subunit, preventing the elongation of peptide chains, and consequently, inhibiting protein synthesis (Chang and Pechère 1998). Spiramycin displays selective toxicity since it is probably not active against eukaryotes (Brisson-Noel et al. 1988). In addition, spiramycin has multifactorial anti-inflammatory properties since it modulates the production of proinflammatory (IL-1, IL-6, IL-8, TNF-α) and anti-inflammatory cytokines (IL-10, possible IL-4), inhibits the formation of leukotriene B4, interferes with the migration and functionality of neutrophils, decreasing oxidant production and apoptosis (Labro 1998; Alzolibani and Zedan 2012). Therefore, the anti-toxoplasmic and anti-inflammatory activities of spiramycin incorporated into PLGA implants contribute not only to reduce the cyst load in acute and chronic ocular infections, but also to modulate the inflammatory process established in the delicate tissues of the eye. The synergistic therapeutic effects of spiramycin can decrease morbidity, and consequently, reduce severe damage to vision.

Spiramycin-loaded PLGA implants were produced by a hot molding technique in which the PLGA softened when heated at a temperature above its *Tg* (61.9 °), providing the formation of monolithic implantable devices in which the drug was homogeneously distributed throughout the polymeric chains. These systems measured approximately 3.00 mm and 0.90 mm in length and diameter, respectively; making it possible to inject these into the posterior segment of the eye through a tiny needle. Importantly, smaller needles are required to induce less pain in patients, less vitreous reflux and reduced changes in ocular pressure (Rodrigues et al. 2011).

Spiramycin-loaded PLGA implants were characterized by several instrumental analytical techniques. The DSC thermogram of implantable devices showed that the glass transition temperature of the PLGA was modified after incorporating the spiramycin, which indicated the existence of chemical interaction between these substances. Other endothermic polymer and drug events were detected; but they were superimposed, which represented the dispersion of spiramycin among the polymeric chains. Furthermore, as the decomposition of polymer and drug was detected at up to 280 °C (Erbetta et al. 2011), it demonstrated that the hot molding technique used to produce the implants did not induce the thermal degradation of these compounds (Fernandes-Cunha et al. 2017). The FTIR spectra of implantable devices demonstrated the overlapping of typical bands of organic groups of spiramycin and PLGA, indicating the miscibility of these substances; and chemical interactions could not be detected. The XRD diffractogram of implantable devices showed evidences of the semi-crystalline structure of the PLGA due to the presence of sharp peaks in this compound; but the broad peak of spiramycin was not detected, probably due to its entrapment among the polymeric chains. On the other hand, since spiramycin has a mesophase amorphous structure, it does not convert to a crystalline state (Van Eeden 2019; Atassi et al. 2016). Hence, the reflection plan of the drug may be preserved after producing the systems. In conclusion, characterization techniques demonstrated the dispersion of spiramycin throughout the polymeric chains of PLGA and the preserved physical stability of PLGA and spiramycin even after the application of the manufacturing technique of implants. In addition, weak chemical interactions between spiramycin and PLGA may exist, such as Van der Walls type links.

The amorphous structure of spiramycin could interfere with its controlled release from PLGA implants due to its increased aqueous solubility (Melo et al. 2020). However, polymeric implants were capable of releasing the amorphous drug in a controlled manner for 42 consecutive days. PLGA implants released the spiramycin in a biphasic pattern. During the first days, implants showed a burst spiramycin release, indicating that the drug diffused from the surface of the implants. Afterwards, the spiramycin was slowed released via a complex delivery mechanism that involved the diffusion of the drug and erosion of the polymeric matrix. A similar release profile was reported by Fernandes-Cunha et al. (2016), who demonstrated that PLGA implants exhibited an initial burst release of the clindamycin followed by a controlled drug release for a prolonged period. This similarity of release profiles of clindamycin and spiramycin from PLGA implants was attributed to the fact that these systems were manufactured by using the same technique (hot molding process), drug-loading was equal to 25% (w/w), and the polymer showed the same morphological modifications after incubation in the medium. As detected by SEM photomicrographs, before incubation in PBS (pH 7.4), PLGA implants as appeared to be a dense mass, in which polymer and drug could not be distinguished; after incubation in PBS (pH 7.4), the implants showed shape deformation, indicating their mass loss, and the surface was covered by fissures. Finally, the release of spiramycin from PLGA implants fit best in the Korsmeyer-Peppas mathematical model with super case II transport mechanism, indicating that the drug release was dominated by a complex process involving diffusion, surface erosion, and disentanglement (Sonawane et al. 2016).

After demonstrating the sustained spiramycin release from PLGA implants, which is essential to constantly expose *Toxoplasma gondii*, aiming at its elimination in an acute or chronic ocular lesion, the *in vitro* biocompatibility of these implantable devices was investigated against the ARPE-19 cells. In this study, the precursors of implants, as well as the hydrolytic degradation products from polymer, were selected to favor ocular biocompatibility (Da Silva et al. 2010). In order to support this expectation of ocular biocompatibility, ARPE-19 cells were cultured in direct contact with spiramycin and polymeric by-products released from PLGA implants. According to the cytotoxicity test, using MTT assay, ARPE-19 cells were not affected by spiramycin and polymeric degradation products released from PLGA implants, suggesting their non-toxicity. This was an important result since minimal levels of damage in mitochondria and mitophagy could trigger cell degeneration. Mitophagy is the mitochondria-specific autophagy by which impaired mitochondria is eliminated to keep normal cellular functions (Wang et al. 2016). Defects in ARPE-19 cell functions may result in damage to vision. Ocular biocompatibility was also investigated regarding the measurement of G0/G1, S, and G2/M phases equivalent to ARPE-19 cell cycle kinetics. According to the flow cytometry, ARPE-19 cell cycle progression was not disturbed by spiramycin and polymeric degradation products released from PLGA implants, indicating that even under a different environment due to the exposition to the drug and lactic and glycolic acids, they did not affect cell proliferation and genome stability (Borland et al. 2018). These data corroborated those obtained by the cell migration test, which demonstrated the ARPE-19 cell capacity to migrate after treated with substances lixiviated from implants. In addition, these substances did not stimulate cell death by apoptosis, which is a complex intracellular process orchestrated by hydrolytic

enzymes, that degrade DNA and cytoskeleton molecules (Verme et al. 2000). Therefore, spiramycin-loaded PLGA implants did not disturb the ARPE-19 cells genetically, morphologically, and biochemically, suggesting their biocompatibility against this cell population, which plays a vital role in keeping retinal functions.
This study also evaluated the ocular biocompatibility of spiramycin-loaded PLGA implants by using the HET-CAM assay. This can substitute the Draize eye test since the chorioallantoic membrane of the chick embryo is similar to the conjunctival tissue of the anterior segment of rabbit eyes. The membrane shows a complete tissue, including blood vessels, which respond to damage though an inflammatory process. To assay with the use of eggs is borderline between *in vitro* and *in vivo* experiments; and ethical approval is not required (Gupta et al. 2010). Spiramycin and polymeric by-products from PLGA implants were investigated by applying this assay; and they showed to be nonirritant, indicating their ocular tolerability. Therefore, data obtained from the HET-CAM assay and the other previously attained with ARPE-19 cells evidenced the non-toxicity of these implants.
Anti-*Toxoplasma* activity of spiramycin-loaded PLGA implants was determined by measuring the MTT metabolization by ARPE-19 cells infected with *Toxoplasma gondii*. Ocular cells in direct contact with spiramycin and degradation products from polymeric implants showed better anti-*Toxoplasma* activity than a pure spiramycin solution, suggesting that drug and lactic and glycolic acids from PLGA exerted synergistic actions against the intracellular parasites. This hypothesis was also described by Fernandes-Cunha et al. (2016), who supposed that clindamycin and the acidity of PLGA degradation products demonstrated better effectiveness against the *Toxoplasma gondii* infecting ARPE-19 cells than pure clindamycin in an aqueous solution. However, this hypothesis should be further studied. Finally, spiramycin-loaded PLGA implants showed their potent activity against *Toxoplasma gondii* without damaging the ARPE-19 cells, which demonstrated their selectivity to intraocular parasites.

4. Experimental

4.1. Development of spiramycin-loaded PLGA implants

Spiramycin and PLGA (85:15 Resomer® RG 858 S, Germany) were dissolved in 5 mL of acetonitrile. The resultant mixture was frozen using nitrogen and lyophilized. The powder was molded into cylindrical implants using a hot plate at approximately 40-45 °C. The spiramycin concentration in PLGA implants was 25% (w/w), which is equivalent to 0.25 mg per implant. Unloaded PLGA implants were also developed. Implants were sterilized by exposure to ultraviolet light for 15 minutes (Fernandes-Cunha et al. 2017).

4.2. Determination of spiramycin content into PLGA implants

The general chapter of the United States Pharmacopoeia was followed (USP 2018). Ten spiramycin-PLGA implants were weighted and the drug into each implant was assayed by using a High-Performance Liquid Chromatographic (HPLC) method previously developed and validated. Chromatographic conditions were: C18 column (150 x 4.6 ODS, 5 µm) at 40 °C; 50 mM phosphate buffer pH 4.26: methanol: acetonitrile (50:35:15) as mobile phase and isocratic elution; 0.8 mL min^{-1} of mobile phase flux; 50 µL of injection volume; detection at 232 nm. The amount of spiramycin was calculated and expressed as the percentage of the pre-indicated value (0.25 mg). The relative standard deviation was also calculated (Souza et al. 2018).

4.3. Characterization

4.3.1. Fourier Transform Infrared Spectroscopy (FTIR)

Infrared spectra were collected in a Fourier Transform Infrared Spectrophotometer (FTIR; Perkin Elmer, model Spectrum 1000). Measurements were carried out using the Attenuated Total Reflectance (ATR) technique. Each spectrum was a result of 32 scans with a resolution of 4 cm^{-1} (Melo et al., 2020).

4.3.2. Powder X-Ray Diffraction (XRD)

Powder X-Ray Diffraction (XRD) was recorded using an X-Ray Diffractometer Shimadzu XRD-7000 (Japan) at 20 °C, 40 kV, 30 mA, and Cu kα radiation at λ = 1,54056 Å, a graphite monocromator. Samples mounted into aluminum sample holders, analyzed at the angle range of 5 up to 35° of 2Θ with a step size of 0.02°, at a rate of 1.2 s. $step^{-1}$, using a pollycapilar focus optics, under spinning of 30 rpm.

4.3.3. Thermal analysis

Thermal behavior was evaluated by Differential Scanning Calorimetry (DSC) and Thermogravimetry (TG)/Differential Thermal Analysis (DTA). DSC curves were obtained in a DSC60 Shimadzu cell, calibrated with Indium (melting point: Tonset = 156.63 °C, ΔHfus = 28.45 $J.g^{-1}$) under dynamic N_2 atmosphere, at 50 mL min^{-1}, heating rate of 10 °C min^{-1}, from 30 to 400 °C, in closed aluminum crucible and sample mass accurately at about 1.5 mg. Thermal phenomena were described by "Tonset " in °C and enthalpy in J g^{-1}. TG/DTA curves were obtained by using a Shimadzu DTG60 thermobalance with a heating rate of 10 °C min^{-1}, from 30 up to 600 °C, dynamic N_2 atmosphere at 50 mL min^{-1}, in an alumina crucible and mass of sample accurately weighted (approximately 2.5 mg) (Melo et al. 2020).

4.3.4. Scanning Electron Microscopy (SEM)

Implants recently produced and submitted to simulated ocular physiological conditions for 60 days were analyzed by using SEM. SEM was performed using a JEOL microscope (model JSM – 6360LV) operating at 15 kV. Implants were fractured and mounted on aluminum stubs using double-sided adhesive tape. Prior to microscopical examination, implants were sputter-coated with a gold layer under argon atmosphere using a sputter apparatus (Balzers Union SCD 040 unit, Germany). Implant surfaces were viewed at 100× and 1000× magnifications; and images were transferred to the computer by means of a Digital Image Transference Interface (DITI). Photomicrographs were adjusted using the software Adobe Photoshop 6.0 and Adobe Illustrator 9.01 (Adobe Systems Incorporated, 2000, USA).

4.4. In vitro release of spiramycin from PLGA implants

In-vitro release of spiramycin was carried out under sink conditions during 60 days. Spiramycin-loaded PLGA implants were immersed in different tubes containing 11.5 mL of phosphate buffer solution (PBS, pH = 7.4) (n = 5). These tubes were incubated at 37 °C and 30 rpm. At predetermined intervals, the release medium was collected and completely renewed with fresh PBS. The amount of spiramycin released from each implant was quantified by a HPLC method. The release profile was evaluated as the cumulative percentage of spiramycin delivered from PLGA implants in the medium. Higuchi, zero order, first order, and Korsmeyer-Peppas mathematical models were applied to evaluate the kinetic profile of spiramycin released from PLGA implants (Fernandes-Cunha et al. 2017).

4.5. In vitro biocompatibility study

4.5.1. ARPE-19 cell culture

ARPE-19 cells, an established but no immortalized human RPE cell line, were grown in Dulbecco's Modified Eagle's Medium and Ham's F12 medium (DMEM/F12 Gibco BRL, USA) with 10% fetal bovine serum (FBS Gibco BRL, USA) in a 37 °C humidified atmosphere of 5% CO_2 and 95% air (Da Silva et al. 2015).

4.5.2. Cytotoxicity of spiramycin released from PLGA implants

After 48 hours in culture, the medium was aspirated, and ARPE-19 cells in contact with the spiramycin and polymeric by-products released from PLGA implants for 4 and 8 days and control TCPS were rinsed with phosphate-buffered saline (PBS). ARPE-19 cells were incubated with 150 µL of 3-[4,5-dimethylthiazol-2-yl]-2,5-diphenyltetrazolium bromide (MTT) (1 mg mL^{-1} in PBS) (Sigma Chemical, USA). After 3 hours of incubation, cells were lysed with 100 µL of isopropanol and absorbance values were measured at 570 nm versus 630 nm using a microplate reader (BioRad, USA). The mean absorbance on the control was set as 100%, while the mean absorbance ± standard deviation obtained with cells in contact with spiramycin and polymeric degradation products was calculated as a percentage of the control. Data were shown as a histogram (Da Silva et al. 2015).

4.5.3. Cell cycle kinetic

5×10^5 ARPE-19 cells were seeded into 12-well plates. After 24 hours, cells were treated with spiramycin and polymeric by-products released from PLGA implants for 4 and 8 days. After 48 hours of treatment, the supernatant was collected and cells were detached using trypsin. They were centrifuged at 1000 rpm for 10 minutes. The sediment was fixed with 70% ethanol and maintained at -20 °C for 12 hours (Brassesco et al. 2013). Subsequently, cells were washed, resuspended in 200 µL of labeling solution (0.0914 g of magnesium chloride; 0.0774 g of sodium citrate; 0.04766 g of HEPES; 10 µL of Triton-X, 0.5 mL of propidium iodide, and 9490 mL of water (Galbraith et al. 1983), placed on ice and protected from light for at least 30 minutes. Percentages of cells in the G0/G1, S and G2/M phases were measured using flow cytometry (BD FACSCalibur) and analyzed using FlowJo® software. Data from 30,000 cells were collected in each file and experiments were conducted in triplicate.

4.5.4. Cell migration (in vitro wound-healing assay)

Cells were seeded onto six-well culture plates (10^6 cells/well) and cultured during 24 h. Cell monolayer was scraped with a sterile 200-µL pipette tip to create a wound. Then, cells were washed and treated with spiramycin and polymeric by-products released from PLGA implants for 4 and 8 days (medium serum-free). After 48 h of treatment, cell migration was observed and images were captured at 0, 48 and 72 h with an inverted microscope. Quantification of cell motility was performed using the software ImageJ measuring the distance between the invading front of cells in three random selected microscopic fields for each condition (Gándara et al. 2014).

4.6. Hen's egg test-chorioallantoic membrane (HET-CAM) irritation test

Fertilized hen's eggs were purchased from a poultry farm (Alimentos Rivelli, Brazil). Collected hen's eggs were incubated at 37±0.5 °C and 40±4% relative humidity for 10 days. Eggs were turned every day during incubation but were left in a horizontal position for several minutes to assure that the embryo was properly positioned. On day 10, each egg was opened by cracking the underside of the egg against the edge of a plastic Petri dish (Alany et al. 2006). CAM was exposed and samples were placed directly onto the CAM's surface (n = 6 for each sample). After 20 seconds, samples were discarded and the CAM was carefully washed with HEPES buffer (pH 7.4) to ensure the total removal of the tested substance. CAM was visually observed for 5 minutes (0.5, 2 and 5 minutes) regarding the appearing of any of the following phenomena: hyperemia, hemorrhage, and coagulation (Sá et al. 2015). Samples were PBS pH 7.4 (negative control), 0.1 mol/L sodium hydroxide solution (positive control), spiramycin and polymeric by-products released from PLGA implants for 4 and 8 days.

4.7. Anti-Toxoplasma activity

Approximately 5×10^4 ARPE-19 cells were seeded in 24-well tissue culture plates 24 h before the assay. Cells in DMEM/F-12 medium were infected with tachyzoites from the virulent RH strain of *Toxoplasma gondii* using a 5:1 parasite – host cell ratio according to a host cell count on the day of infection. Plates were gently centrifuged (1000 rpm for 2 min) to allow immediate contact of tachyzoites with host cells. Tachyzoites were allowed to interact for 1 h, cell monolayer was washed twice with PBS to remove non-adhered parasites and 1 mL of the basal medium was added to each well. Different treatments were added to infected cells in triplicate and corresponded to spiramycin aqueous solution at 0.25 mg, spiramycin and polymeric by-products released from PLGA implants for 4 and 8 days. After 24 h, the medium was removed and 170 µL of MTT solution (5 mg mL^{-1}) and 210 µL of new basal medium were added to each well. Two hours later, formazan crystals were dissolved with 210 µL of SDS-10% in HCl. After 18 h, 100 µL of solution was transferred to a 96-well plate, and the optical density was measured at 595 nm. Cells not infected with tachyzoites were subjected to the same procedure, as a control. Cell death control was assayed by culturing cells/tachyzoites with staurosporine (200 µM) (Fernandes-Cunha et al. 2016).

4.8. Statistical analysis

Results were expressed as mean±standard deviation. Data were tested for normality and investigated for statistical significance using one-way analysis of variance (ANOVA), when appropriate. A p-value of less than 0.05 was considered significant.

Acknowledgements: This work was supported by the CNPq [grant number 302671/2018-8] (Brasília, Brazil), CAPES (Brasília, Brazil), FAPEMIG (Minas Gerais, Brazil), UFOP (Minas Gerais, Brazil), and UFSJ (Minas Gerais, Brazil). Authors thank Mrs. Rosálida Estevam Nazar Lopes and Prof. Ricardo Wagner de Almeida Vítor for the donation of the *Toxoplasma gondii* strain.

Conflict of interest: None declared.

References

Alany RG, Rades T, Nicoll J, Tucker IG, Davies NM (2006) W/O microemulsions for ocular delivery: evaluation of ocular irritation and precorneal retention. J Control Rel 111: 145–152.

Alzolibani AA, Zedan K (2012) Macrolides in chronic inflammatory skin disorders. Mediators Inflamm 2012: 159354.

Atassi F, Behme RJ, Patel PJ (2016) Mesomorphous versus traces of crystallinity: the itraconazole example. Thermochim Acta 574: 133–139.

Borland D, Yi H, Grant GD, Kedziora KM, Chao HX, Haggerty RA, Kumar J, Wolff SC, Cook JG, Purivs JE (2018) The cell cycle browser: an interactive tool for visualizing, simulating, and perturbing cell-cycle progression. Cell Syst 7: 180–184.

Brassesco MS, Pezuk JA, Morales AG, De Oliveira JC, Roberto GM, Da Silva GN, Francisco HO, Scrideli CA, Tone LG (2013) In vitro targeting of Polo-like kinase 1 in bladder carcinoma: comparative effects of four potent inhibitors. Cancer Biol Ther 14: 648–657.

Brisson-Noël A, Trieu-Cuot P, Courvalin P (1988) Mechanism of action of spiramycin and other macrolides. J Antimicrob Chemother 22(B): 13–23.

Brydak-Godowska J, Moneta-Wielgoś J, Kęcik D, Borkowski PK (2015) Management of toxoplasmic retinochoroiditis during pregnancy, postpartum period and lactation: clinical observations. Med Sci Monit 21: 598–603.

Chang HR, Pechère JCF (1988) Activity of spiramycin against Toxoplasma gondii in vitro, in experimental infections and in human infection. J Antimicrob Chemother 22(B): 87–92.

Da Silva GR, Lima TH, Oréfice RL, Fernandes-Cunha GM, Silva-Cunha A, Zhao M, Behar-Cohen F (2015) In vitro and in vivo ocular biocompatibility of electrospun poly(ε-caprolactone) nanofibers. Eur J Pharm Sci 20: 9–19.

Da Silva MG, Cardoso JF, Perasoli FB, Branquinho RT, Mourão RS, Tavares HS, Xocaira MLCT, Guimarães DSM, Viana GHR, Varotti FP, Da Silva GR (2020) Nanoemulsion composed of 10-(4,5-dihydrothiazol-2-yl)thio)decan-1-ol), a synthetic analog of 3-alkylpiridine marine alkaloid: development, characterization, and antimalarial activity. Eur J Pharm Sci 151: 105382.

De Souza LF, Maia KN, Patrício PSO, Fernandes-Cunha GM, Da Silva MG, Jensen CEM, Da Silva GR (2016) Ocular inserts based on chitosan and brimonidine tartrate: Development, characterization and biocompatibility. J Drug Deliv Sci Tec 32(A): 21–30.

Dubey JP, Jones JL (2008) Toxoplasma gondii infection in humans and animals in the United States. Int J Parasitol 38: 1257–1278.

Erbetta CDC, Viegas CCB, Freitas RFS, Sousa RG (2011) Synthesis and thermal and chemical characterization of the poly(D,L-lactide-co-glycolide) copolymer. Polímeros 21: 376–382.

Fernandes-Cunha GM, Fialho SL, Da Silva GR, Silva-Cunha A, Zhao M, Behar-Cohen F (2017) Ocular safety of Intravitreal Clindamycin Hydrochloride Released by PLGA Implants. Pharm Res 34: 1083–1092.

Fernandes-Cunha GM, Rezende CM, Mussel WN, Da Silva GR, Gomes EC, Yoshida MI, Fialho SL, Goes AM, Gomes DA, de Almeida-Vitor RW, Silva-Cunha A (2016) Anti-Toxoplasma activity and impact evaluation of lyophilization, hot molding process, and gamma-irradiation techniques on CLH-PLGA intravitreal implants. J Mater Sci Mater Med 27: 1–12.

Galbraith DW, Harkins KR, Maddox JM, Ayres NM, Sharma DP, Firoozabady E (1983) Rapid flow cytometric analysis of the cell cycle in intact plant tissues. Science 220: 1049–1051.

Gándara L, Sandes E, Di Venosa G, Prack Mc Cormick B, Rodriguez L, Mamone L, Batlle A, Eiján AM, Casas A (2014) The natural flavonoid silybin improves the response to photodynamic therapy of bladder cancer cells. J Photochem Photobiol B 133: 55–64.

Garweg JG (2016) Atrophy of the macula in the context of its wet, age-related degeneration: an inescapable consequence of anti-VEGF therapy? Ophthalmologe 113: 1036–1045.

Gupta H, Aqil M, Khar RK, Ali A, Bhatnagar A, Mittal G (2018) Sparfloxacin-loaded PLGA nanoparticles for sustained ocular drug delivery. Nanomed Nanotechnol 6: 324–333.

Gote V, Sikder S, Sicotte J, Pal D (2019) Ocular drug delivery: present innovations and future challenges. J Pharmacol Exp Ther 370: 602–624.

Holland GN, Lewis KG (2002) An update on current practices in the management of ocular toxoplasmosis. Am J Ophthalmol 134: 102–114.

Khine KT, Albini TA, Lee RK (2020) Chronic retinal detachment and neovascular glaucoma after intravitreal stem cell injection for Usher Syndrome. Am J Ophthalmol 18: 100647.

Kim SJ, Scott IU, Brown GC, Brown MM, Ho AC, Ip SM, Recchia FM (2013) Interventions for toxoplasma retinochoroiditis: a report by the American Academy of Ophthalmology. Ophthalmology 120: 371–378.

Konstantinovica N, Guegan N, Stäjner T, Belaz S, Robert-Gangneux F (2019) Treatment of toxoplasmosis: Current options and future perspectives. FAWPAR 15: e00036.

Labro MT (1998) Anti-inflammatory activity of macrolides: a new therapeutic potential? J Antimicrob Chemother 41(B): 37–46.

Lasave AF, Díaz-Llopis M, Muccioli C, Belfort Jr R, Arevalo JF (2010) Intravitreal Clindamycin and Dexamethasone for Zone 1 Toxoplasmic Retinochoroiditis at Twenty-Four Months. Ophthalmology 117: 1831–1838.

Maenz M, Schluter D, Liesenfeld O, Schares G, Gross U, Pleyer U (2014) Ocular toxoplasmosis past, present and new aspects of an old disease. Prog Retin Eye Res 39: 77–106.

Melo CM, Cardoso JF, Perasoli FB, Neto ASO, Pinto LM, de Freitas-Marques MB, Mussel WN, Magalhães JT, Moura SAL, Araújo MGF, Da Silva GR (2020) Amphotericin B-loaded Eudragit RLl100 nanoparticles coated with hyaluronic acid for the treatment of vulvovaginal candidiasis. Carbohydr Polym 230: 115608.

Ozgonul C, Besirli CG (2017) Recent developments in the diagnosis and treatment of ocular toxoplasmosis. Ophthalmic Res 57: 1–12.

Pappas G, Roussos N, Falagas ME (2009) Toxoplasmosis snapshots: global status of Toxoplasma gondii seroprevalence and implications for pregnancy and congenital toxoplasmosis. Int J Parasitol 39: 1385–1394.

Pascual-Pasto G, Olaciregui NG, Opezzo JAW, Castillo-Ecija H, Cuadrado-Vilanova M, Paco S, Rivero EM, Vila-Ubach M, Restrepo-Perdomo CA, Torrebadell M, Suñol M, Schaiquevich P, Mora J, Bramuglia GF, Chantada GL, Carcaboso AM (2017) Increased delivery of chemotherapy to the vitreous by inhibition of the blood-retinal barrier. J Control Rel 264: 34–44.

Petersen E, Kijlstra A, Stanford M (2012) Epidemiology of ocular toxoplasmosis. Ocul Immunol Inflamm 20: 68–75.

Robert-Gangneux F, Dardé ML (2012) Epidemiology of and diagnostic strategies for toxoplasmosis. Clin Microbiol Rev 25: 264–296.

Rodrigues EB, Grumann A, Penha FM, Shiroma H, Rossi E, Meyer CH, Stefano V, Maia M, Magalhaes O, Farah ME (2011). Effect of needle type and injection technique on pain level and vitreal reflux in intravitreal injection. J Ocul Pharmacol Ther 27: 197–203.

Sá FA, Taveira SF, Gelfuso GM, Lima EM, Gratieri T (2015) Liposomal voriconazole (VOR) formulation for improved ocular delivery. Colloid Surface B 1(133): 331–338.

Saliba JB, Vieira S, Fernandes-Cunha GM, Da Silva GR, Fialho SL, Silva-Cunha A, Bousquet E, Naud MC, Ayres E, Oréfice RL, Tekaya M, Kowalczuk L, Zhao M, Behar-Cohen F (2016) Anti-inflammatory effect of dexamethasone controlled released from anterior suprachoroidal polyurethane implants on endotoxin-induced uveitis in rats. Invest Ophthalmol Vis Sci 57: 1671–1679.

Silva GR, Silva-Cunha A, Behar-Cohen F, Ayres E, Oréfice RL (2010) Biodegradation of polyurethanes and nanocomposites to non-cytotoxic degradation products. Polym Degrad Stabil 95: 491–499.

Sonawane SJ, Kalhapure RS, Rambharose S, Mocktar C, Vepuri SB, Soliman M, Govender T (2016) Ultra-small lipid-dendrimer hybrid nanoparticles as a promising strategy for antibiotic delivery: In vitro and in silico studies. Int J Pharm 504: 1–10.

Souza RO, Lima TH, Oréfice RL, Araújo MGF, Moura SAL, Magalhães JT, Silva GR (2018) Amphotericin B-Loaded Poly(lactic-co-glycolic acid) Nanofibers: an alternative therapy scheme for local treatment of vulvovaginal candidiasis. J Pharm Sci 107: 2674–2685.

Tabuenca LB, Heras HM, Mozo MC, Fanlo PM, Compains ES (2019) Intravitreal clindamycin as a therapeutic alternative in severe ocular toxoplasmosis. Arch Soc Esp Oftalmol (English Edition) 94: 602–604.

Tamaddon L, Mostafavi SA, Karkhane R, Riazi-Esfahani M, Dorkoosh FA, Rafiee-Tehrani M (2015) Thermoanalytical characterization of clindamycin-loaded intravitreal implants prepared by hot melt extrusion. Adv Biomed Res 27: 147.

USP – United States Pharmacopeial Convention (Ed.) (2018) United States pharmacopeia (41st ed.). Rockville.

Van Eeden R (2019) The physico-chemical properties of spiramycin and clarithromycin. (Potchefstroom: North-West University). (Dissertation- Doctoral).

Vermes I, Haanen C, Reutelingsperger C (2000) Flow cytometry of apoptotic cell death. J Immunol Methods 243: 167–190.

Wang X, Yang H, Yanagisawa D, Bellier JP, Morino K, Zhao S, Liu P, Vigers P, Tooyama I (2016) Mitochondrial ferritin affects mitochondria by stabilizing HIF-1α in retinal pigment epithelium: implications for the pathophysiology of age-related macular degeneration. Neurobiol Aging 47: 168–179.

Xiaoli L, Pingping Y (2018) Early diagnosis and successful treatment of acquired toxoplasmosis infectious retinochoroiditis: A case report. Medicine 97: e11231.